A solar photocatalytic floating reactive barrier for aqueous gas emissions interception and treatment

Jeffrey T. Martin,[a] Timothy M. C. Leshuk,[a,b] Brad Wilson,[a,c] Aaron Cheung,[a] Zachary W. Young,[a] Frank Gu*[,a,b]

[a]H2nanO Inc., Kitchener, Ontario, Canada, N2G 1H6
[b]Department of Chemical Engineering and Applied Chemistry, University of Toronto, Toronto, Ontario, Canada, M5S 3E5
[c] Stantec, 100-300 Hagey Boulevard, Waterloo, ON, Canada, N2L 0A4
*frank@h2nano.ca; f.gu@utoronto.ca

Abstract

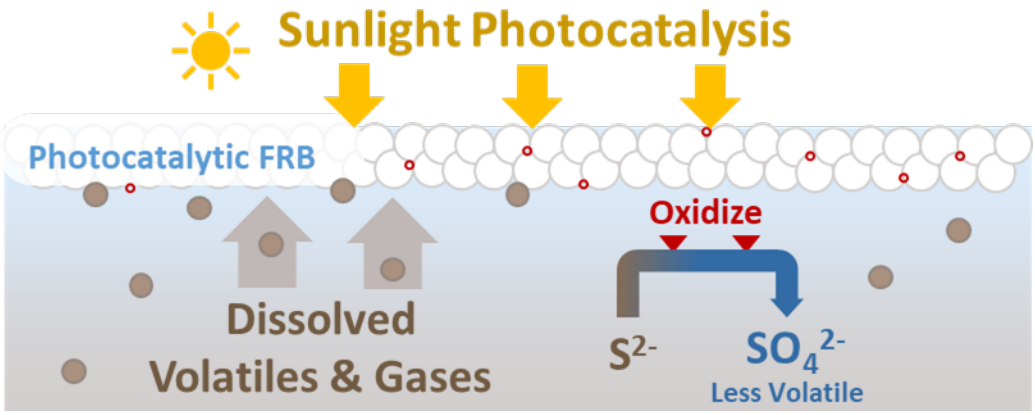

Reduced sulfur compounds produced as a by-product of anaerobic digestion pose a significant health and environmental hazard for nearby communities. Here we assessed a novel floating reactive barrier (FRB), comprised of buoyant photocatalysts (BPCs), as a passive solution to intercept and treat malodorous compounds before crossing the air-water interface. Using industry provided samples of oil sands process water (OSPW) containing anaerobically produced aqueous sulfide, the FRB system was evaluated at both the bench and pilot scale. The photocatalytic FRB demonstrated a 95% reduction in H_2S emissions at the lab scale and up to 98% at the pilot-scale under outdoor weather conditions and natural sunlight. H_2S emissions intercepted by the FRB were found to be oxidized to non-volatile sulfate. An empirical reactive transport model describing the performance of the FRB is proposed informed by the results obtained in this work. The photocatalytic FRB described herein is proven to be an effective measure for the mitigation of potentially hazardous reduced sulfur compound emissions under solar UV conditions.

Synopsis

A novel photocatalytic floating reactive barrier was validated for the interception and passive solar treatment of aqueous H_2S emissions from anerobic tailings pond water.

Keywords

photocatalysis, passive treatment, H_2S, reduced sulfur compounds, floating reactive barrier, transport model

1.0 Introduction

The removal of reduced sulfur compound (RSC) emissions from anaerobic digestion poses substantial health hazards and corrosion maintenance issues [1]. RSC emissions hazards can originate from a variety of sources including aquifers contaminated by abandoned oil and gas wells [2], [3], municipal wastewater systems [1], agricultural wastewater [4]–[7], and mining tailings ponds [8]. For Canada's Oil Sands mining tailings ponds, residual diluent in the tailings undergoes simultaneous sulfidogenesis and methanogenesis in the mature fine tailings (MFT) layer [8]–[13]. Currently methane and other volatile organic carbons (VOCs) represent the majority of emissions from these tailings ponds [8], [9], but the convective transport of methane from the MFT to the tailings pond surface can act as a carrier for malodourous sulfur emissions (H_2S) [11], [13], circumventing the natural sulfur cycle in the pond. These RSC emissions may affect the local air quality and pose a potential health risk to nearby communities and operators [14]–[16]. Removing RSC emissions is a relevant environmental and health issue, yet due to the scale of these systems, effective treatment of large aqueous sources is a challenge that is not effectively addressed by conventional technologies.

Photocatalysis has previously been studied as an effective method for the elimination of H_2S and other malodorous compounds from air sources [17]–[24]. These past studies focused on treatment of gaseous H_2S emissions where interception and containment are more difficult. Photocatalytic treatment of H_2S in the aqueous phase prior to volatilization has yet to be investigated. Previous work has validated the efficacy of using floating photocatalysts as a passive advanced oxidation process (p-AOP) for the treatment of environmentally persistent naphthenic acids in mining process-affected water using natural sunlight UV-radiation at the bench-scale [25], [26]. The photocatalyst is immobilized on a buoyant substrate and naturally concentrated at the air-water interface for optimal sunlight intensity. Due to the cohesive and self-distributing nature of these buoyant photocatalysts they form a floating layer upon deployment that simultaneously acts as a physical barrier to volatile compounds while performing oxidative photocatalytic treatment.

This floating reactive barrier (FRB) is analogous to the permeable reactive barriers currently used as an in-situ treatment method for groundwater remediation [27], [28] and is expected to have a significant impact on the management of fugitive emissions and malodorous compounds. As the FRB is fully wetted, the odour compounds are expected to diffuse through the photocatalyst layer while still contained in the aqueous phase. Solute transport through the layer is driven primarily by diffusion rather than convection (Pe = 7.5*10^-5, calculation in SI). The transport rate of volatile compounds is slowed by the tortuosity of the layer and by the photocatalytic media producing radical species (superoxide and hydroxyl radicals) that oxidize the reduced emission compounds during the diffusive process. This paper presents the FRB as a novel mechanism for the interception and treatment of volatile emissions from aqueous sources at the air-water interface. The work herein presents results from both bench and pilot-scale treatment of naturally occurring H_2S emissions from an industry effluent. Additionally, a steady-state reactive transport model through the FRB layer is proposed using parameters derived from experimental data. The hypotheses of this study were to demonstrate that a photocatalytic FRB can provide simultaneous vapour barrier and treatment of volatile sulfides and to confirm that these principles are maintained under typical operating conditions at a larger scale (natural sunlight, weather effects, bubbling).

2.0 Floating Reactive Barrier Mass Transfer Model

To elucidate the mechanism describing volatile transport through the floating reactive barrier (FRB), a mass transfer model is proposed using a one-dimensional form of the diffusion-reaction equation, which for a 1st order photocatalytic reaction in homogeneous porous media is described by:

$$\frac{\partial c}{\partial t} = D\frac{\partial^2 c}{\partial x^2} - kIc = D\frac{\partial^2 c}{\partial x^2} - k'c$$

where *c* is the concentration of the solute, *D* is the diffusivity of the solute through the FRB, *k* is the apparent first order rate constant for the photocatalytic oxidation of the solute, and *I* is the irradiance applied to the FRB. This model implements pseudo-first order kinetics as is typically applied to photocatalytic treatment of low-concentration contaminants (ppb to ppm range) and justified by the Langmuir-Hinshelwood kinetics model [29]–[35] (Figure S2 and Table S2). For this model it is assumed that there is no convective transport across the FRB and that mass transfer through the layer is governed by diffusion (Pe = 7.5*10^-5). It is also assumed that the diffusion coefficient and UV irradiation is uniform across the layer and that there are negligible mass transfer limitations from the bulk liquid to the liquid-FRB interface. At steady state $\frac{\partial c}{\partial t} = 0$ and Equation (1) is in the form of a second order linear ODE with a solution of:

$$c(x) = C_1 e^{\left(\sqrt{\frac{k\prime}{D}}x\right)} + C_2 e^{\left(-\sqrt{\frac{k\prime}{D}}x\right)}.$$

Using the boundary conditions of $c(0) = c_0$ and $c'(\delta) = 0$, where δ is the thickness of the FRB layer, the constants C_1 and C_2 can be solved for:

$$C_1 = \frac{c_0}{\left(1+e^{\left(2\sqrt{\frac{k\prime}{D}}\delta\right)}\right)}, C_2 = \frac{c_0 e^{\left(2\sqrt{\frac{k\prime}{D}}\delta\right)}}{\left(1+e^{\left(2\sqrt{\frac{k\prime}{D}}\delta\right)}\right)}.$$

Given a sufficient combination of a relatively small diffusivity, a large FRB layer thickness, and a large reaction coefficient, the FRB system can effectively mitigate volatile emissions across the barrier. The diffusivity of a particular species in the FRB layer can be derived experimentally using both aqueous and gaseous data for a steady state system with negligible reaction (Supporting Information). Additionally, once the diffusivity is known the first-order reaction rate constant within the FRB layer can be derived from experimental data (Table S3). This model provides a useful methodology with which to quantify these difficult to measure properties that are essential parameters governing the efficacy of the photocatalytic FRB.

3.0 Methods

3.1 Lab-scale closed-cell reactor

3.1.1 Photocatalysis experiments

A solution of 1.5 L of pH-adjusted Oil Sands process water (OSPW), sourced from an industry partner and preserved at pH 10 with NaOH (Fisher Scientific, ≥ 97%, ACS certified), was added to a glass cylindrical closed-cell reactor (2.5 L total volume and cross-sectional area of 0.0175 m^2) (Figure 1). A pre-measured

amount of photocatalyst composite powder was added to the surface of the water to achieve a catalyst layer thickness of approximately 0.5 - 1.0 cm across the edge to centre of the reactor. Prior to treatment, the headspace volume was purged tenfold at a flow rate of 300 mL/min using compressed air. Gaseous headspace samples were collected using compressed air flow through a 1% NaOH solution midget impinger apparatus at the outlet of the reactor, capturing any H_2S or SO_2 present. H_2S and SO_2 were then analyzed in the 1% NaOH solution using the aqueous sulfide and sulfite methods described below. Following the headspace sample, 20 mL of an aqueous sample was taken using a gas-tight glass syringe for total sulfide, sulfite, and sulfate analysis. The reactor was exposed to UV-A light (Philips F20T12/BL, peak emission 350 nm, Figure S1) at an intensity of 3.15 mW/cm^2 for 120 h. No agitation was used during the experiment. Additional information on the methods used can be found in the supplementary material.

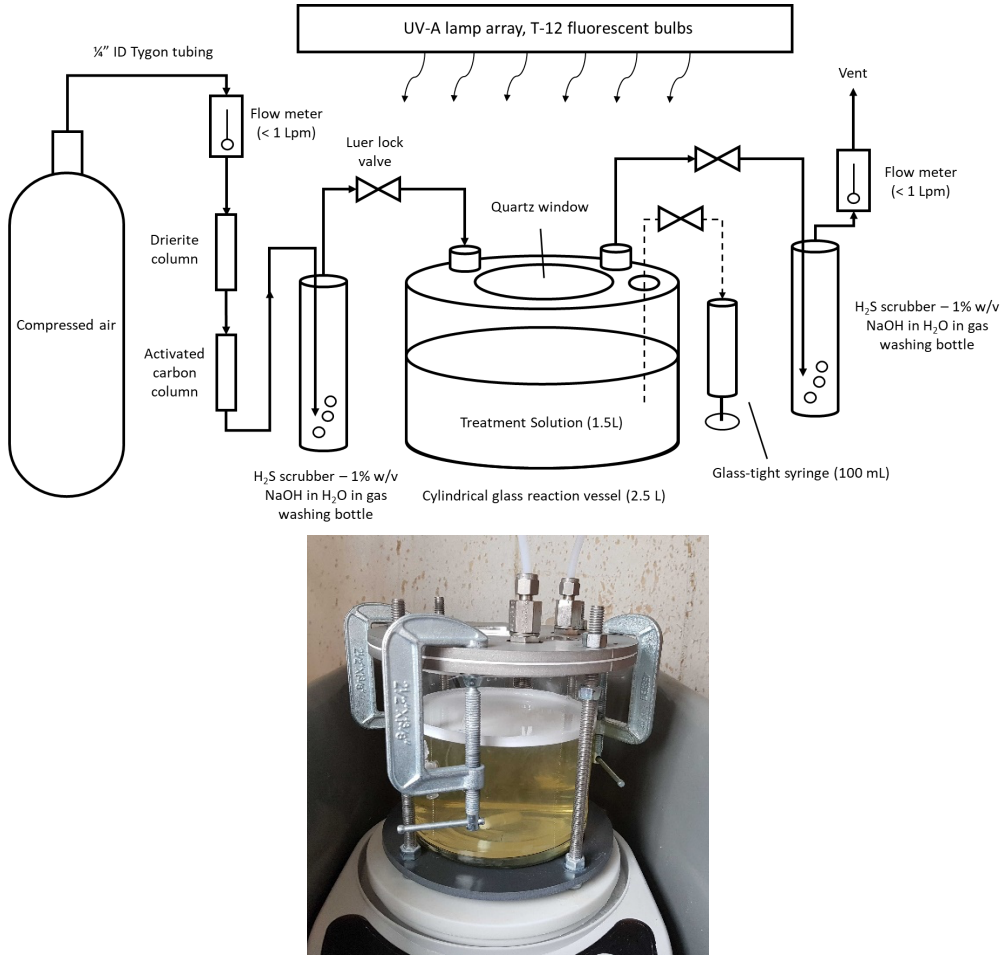

Figure 1 - Lab-scale Photocatalytic Reactor Setup

The total aqueous sulfide and H_2S scrubber solution were analyzed using a methylene blue colorimetric test according to the standard method for total sulfides [36]. Aqueous sulfite was measured according to a colorimetric test referenced from established protocols in literature [37], [38]. Sulfate was analyzed using a standard turbidimetric method [39]. Sample analysis was performed on the same day as sampling. The total aqueous sulfur content was analyzed using inductively coupled plasma optical emission spectrometry (ICP-OES) and the remaining balance between the ICP-OES results and the combined S^{2-}, SO_4^{2-}, SO_3^{2-}, and H_2S species was recorded as a sulfur oxidation intermediate (SOI), similar to the method

reported in [40]. The UV intensity was measured at the quartz glass using a UVA/B light meter (Sper Scientific, NIST certified calibration). The volumetric UV dose was determined based on the UV intensity measured at the quartz glass multiplied by the window area and the reaction time, and then normalized by the solution volume.

3.2 Field-Scale Closed Cell Reactor

3.2.1 Treatment and Emissions Experiments

The first phase of outdoor demonstrations was designed to test treatment at an increased scale, using a solar UV-light source, and exposure to environmental variabilities in outdoor conditions. A closed headspace was initially used for accurate characterization of the gas phase. OSPW used in these experiments was sourced from an industrial partner. Due to air oxidation during transport, the OSPW samples arrived with aqueous sulfide concentrations of 0.6-0.7 mg/L. Prior to the experiments the OSPW was dosed with $Na_2S{\cdot}9H_2O$ to achieve the target initial sulfide concentration of 16-26 mg/L S^{2-} at pH of 8-8.8.

Field-scale experiments used a custom closed cell reactor (CCR) constructed from a 650 L capacity polypropylene tank with a UV-transparent acrylic lid (Figure 2). 530 L OSPW was added to each reactor (60 cm depth) prior to dosing with a catalyst layer thickness of 0.2-1 cm. Headspace H_2S concentrations were measured using a Ventis MX4 handheld gas meter with a 0 - 500 ppm_v range (Industrial Scientific). Gaseous sampling was conducted through direct headspace measurements at 3–4-hour intervals. Aqueous samples were periodically collected using 50 mL syringes from sampling ports in the reactor. Aqueous sulfide concentration was analysed according to a standard method for total dissolved sulfides [36] using a Hach DR-900 colorimeter kit. Additionally, each CCR was outfitted with a pH sensor (Atlas Scientific ENV-50-pH), a UV-light sensor (sglux UV-Cosine), a headspace humidity and temperature probe (Dwyer RHP-2D11), a liquid thermocouple (ProSense THMJ-C12-01), liquid (OMEGA PX119-015GI) and headspace (Dwyer Mark II 25) pressure sensors, a vacuum breaker (Plast-O-Matic VBM050EP-PV), and a mixing pump (Grundfos 99452459).

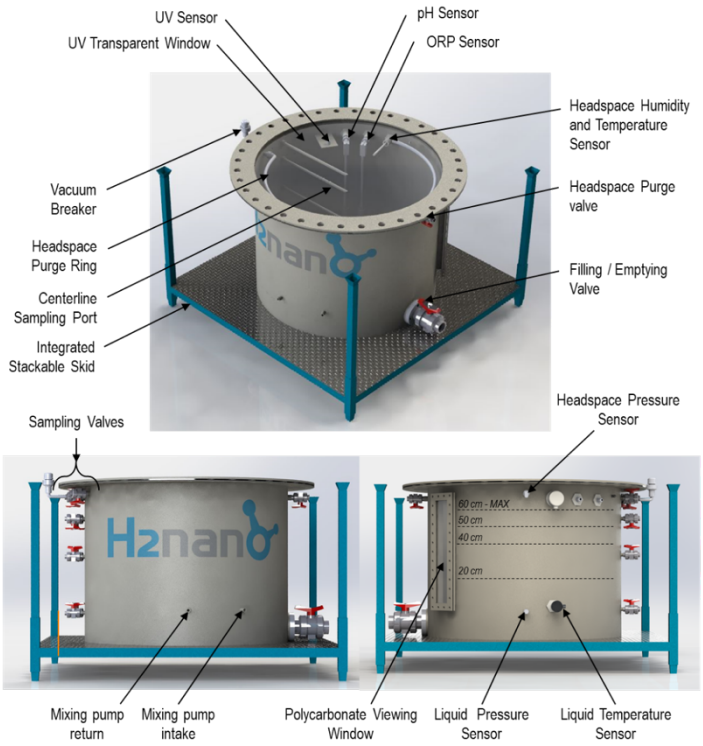

Figure 2 - Conceptual render of the field-scale closed cell reactor completed during design and sizing phase.

3.3 Open tank system

For the open-air experiments, a second OSPW shipment was dosed with $Na_2S{\cdot}9H_2O$ to an elevated initial sulfide concentration of 99.6 mg/L S^{2-}. The open-air reactor tank was filled with OSPW to 60 cm depth with an open surface area of 30 m^2. In accordance with the closed-cell reactor experiments an FRB layer thickness of 0.2-1 cm was used. Time-based gaseous H_2S measurements were collected every 5 min from a 450 mm stainless steel flux chamber (Scentroid Model #SF450; 0.156 m^2 area) which was flushed with compressed air to a hand-held H_2S meter (Ventis MX-4). The open tank system with buoyant photocatalyst and the flux chamber are displayed below in Figure 3.

Figure 3 – Open tank FRB system using a flux chamber (left) and buoyant photocatalyst (right)

4.0 Results and Discussion

4.1 Lab-Scale Treatment Results

The objective of these initial proof-of-concept experiments was to demonstrate the vapour barrier and photocatalytic treatment effects of the FRB system for targeting H_2S in OSPW at the lab-scale. To validate the barrier effects, the floating permeable reactive barrier performance was compared to a dark control (no UV, no photocatalyst barrier), an adsorption control (no UV, with photocatalyst barrier), and a UV control (UV, no photocatalyst barrier).

Analyzing the cumulative H_2S released into the photoreactor headspace, a 95 % reduction in H_2S emissions was observed when compared to the dark control (no catalyst, no UV), validating the barrier properties of the FRB layer at the lab scale (Figure 4a). The efficacy of the photocatalytic FRB to prevent and eliminate H_2S was further validated when compared to a non-reactive barrier (FRB but no photocatalytic activity due to the absence of UV) and bare UV-illuminated surface controls, reducing the cumulative H_2S emissions by 84% and 87%, respectively. Additionally, although large discrepancies were observed between replicates (n=2), in the absence of UV irradiation the FRB was able to block H_2S emissions by 71% when compared to a non-illuminated bare surface. Therefore, even during periods of low solar irradiance the FRB layer can still reduce H_2S emissions. It was observed that the majority of H_2S emissions occurred within the first 24-48 h of each experiment, including in the presence of the FRB layer. This phenomenon was likely due to the high volatility of H_2S gas and a greater driving force for transfer to the headspace that was reduced over time due to photocatalytic and air oxidation.

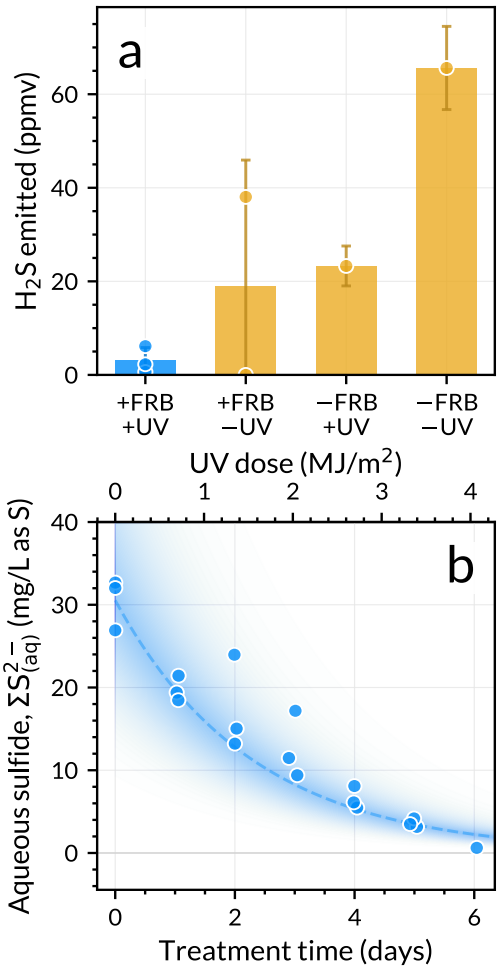

Figure 4 – a) Cumulative H_2S release measured in the photoreactor headspace (6-day experiment duration). Error bars represent pooled test replicate variance (n=3 for BPC layer experiments) and analytical method uncertainty. Dots indicate individual replicate measurements for each series. b) Photocatalytic degradation of aqueous sulfide in OSPW under the BPC layer. Error bars represent pooled test replicate variance (n=3) and analytical method uncertainty.

In addition to the volatile barrier properties demonstrated in the previous section, the FRB layer degraded aqueous sulfide from an initial concentration of 30.5 mg/L to 3.6 mg/L via photocatalysis within 120 h of simulated sunlight exposure (42.7 kJ/L cumulative UV exposure) (Figure 4b). Pseudo-first order reaction kinetics were observed with a rate constant of 0. 487 ± 0.055 days^{-1} (0.158 ± 0.018 m^2/MJ based on surface area UV dose). Although no mixing was used during these tests, the OSPW cap layer in oil sands tailings ponds is well mixed by wind, wave, [41]–[43] and methanogenic bubbling activity [9], [44]. It is expected that under these natural mixing conditions the sulfide treatment rate for the FRB will increase significantly due to increased mass transfer of sulfide from the bulk OSPW cap layer to the catalyst layer.

4.1.1 Sulfide Treatment Speciation

Additional sulfide treatment experiments were performed to elucidate the sulfur compound speciation during photocatalytic FRB treatment under controlled lab-scale conditions. Due to interference caused by

the OSPW sulfate background levels (190-350 mg/L), a synthetic OSPW matrix was used (Table S1). The simulated OSPW was dosed with sodium sulfide to an initial concentration of 300 mg/L sulfide and no sulfate was added so that any sulfate detected would be a product of the oxidative sulfide treatment. To complete the sulfur mass balance, total aqueous sulfur, S^{2-}, SO_4^{2-}, SO_3^{2-}, and H_2S were individually quantified using the methods outlined in Section 3.

The results of the sulfur speciation measured during photocatalytic treatment and in a dark control are compared below in Figure 5 respectively. During photocatalysis, the total aqueous sulfur content remained constant at 367.1 ± 20 mg/L, indicating limited loss of volatile sulfur compounds during treatment. Notably, the photocatalytic oxidation of sulfur was fully oxidized to sulfate, with minimal H_2S detected in the headspace. During photocatalysis, various intermediates were formed including sulfite and additional unidentified SOI species ($S_nO_x^{2-}$ thiosalts). These intermediates were found to further oxidize to sulfate and given an increased UV dose, it is predicted that the only sulfur species present would be sulfate. These intermediates were not directly quantified as part of this study due to the highly complex nature of the SOI species and uncertainty over the particular SOI species present.

Comparatively, for the dark control the total aqueous sulfur concentration was 374.5 ± 43 mg/L and appeared to decrease over time. This decrease could be a result of increased transfer of volatile sulfur compounds (H_2S) to the reactor headspace that weren't accounted for by the H_2S measurements. In the dark control, sulfide degradation occurred due to air oxidation, however, only 10% of the total sulfur present as sulfide was fully converted to sulfate. Unlike in the photocatalysis experiment, the SOI species produced were not converted to sulfate during the duration of the experiment, indicating only a partial oxidation of sulfide due to air. Due to the high surface area of the air-water interface compared to the liquid volume, the bulk conversion of aqueous sulfide by oxygen is unlikely to occur at this rate in a full-scale tailings pond and it is expected that the photocatalytic treatment rate (surface-limited) provides a more accurate representation of sulfide oxidation at scale. Treatment of aqueous sulfides was approximately 2x faster in the photocatalytic experiment than the control, demonstrating superior treatment kinetics at elevated sulfide concentrations. The results of these lab-scale investigations validate the reactive barrier properties of the buoyant photocatalytic barrier system, with full elimination of aqueous sulfides and superior retention of H_2S in the aqueous phase when compared to controls.

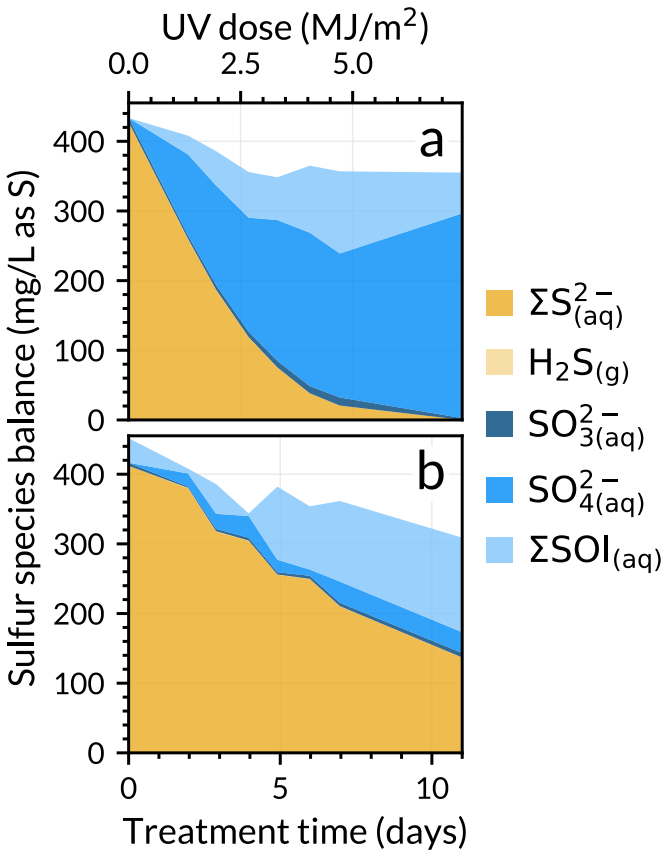

Figure 5 – Sulfur mass balance for the FRB treatment experiment (a) and for a dark control (no catalyst, no UV) (b) using sulfide-spiked simulated OSPW (initially containing no sulfate) confirms reaction mechanism. Continuous UV intensity of 3.02 mW/cm^2, cumulative dose of 2.87 kJ/cm^2. SOI fraction represents unresolved oxidation intermediates. S^{2-} fraction represents all aqueous sulfide species (H_2S, HS^-, and S^{2-}).

4.2 Field-Scale Treatment Results

4.2.1 CCR Emissions Reduction Validation

The objective for the pilot-scale experiments was to demonstrate treatment at a more realistic scale under natural sunlight and weather conditions. Four closed-cell reactors were set up, one control and three FRB reactors, to accurately track the gas-phase accumulation of volatile sulfides. H_2S headspace concentration data for the control reactor is presented as the daily average whereas for the FRB rectors it is presented as the daily average across all three FRB reactors.

Under natural sunlight exposure, the photocatalytic FRB was able to successfully reduce the H_2S emissions from OSPW by 83% to 97% compared to the control (Figure 6). Notably, daily fluctuations in the H_2S emissions occur and are likely due to diurnal temperature fluctuations of up to 6 °C, promoting an increased transfer of H_2S from the aqueous to gas phase during higher temperatures.

While containing up to 97% of the total H_2S emissions, the aqueous sulfide concentration in the FRB reactors was degraded from an initial average concentration of 22.81 mg/L to 6 mg/L during the experiment duration (**Error! Reference source not found.**). Similar to the lab-scale treatment results,

pseudo-first order kinetics were observed with an aqueous sulfide treatment rate of 0.193 ± 0.019 $days^{-1}$ (0.254 ± 0.025 m^2/MJ based on surface area UV dose). The aqueous sulfide treatment rate in the field-scale reactor was notably greater than the lab-scale treatment rate. This increased treatment rate is likely due to increased thermally induced mass transfer in the field-scale reactors due to diurnal temperature fluctuations of up to 6 °C, while the lab-scale reactors were maintained at a constant temperature (19 °C ± 1°C).

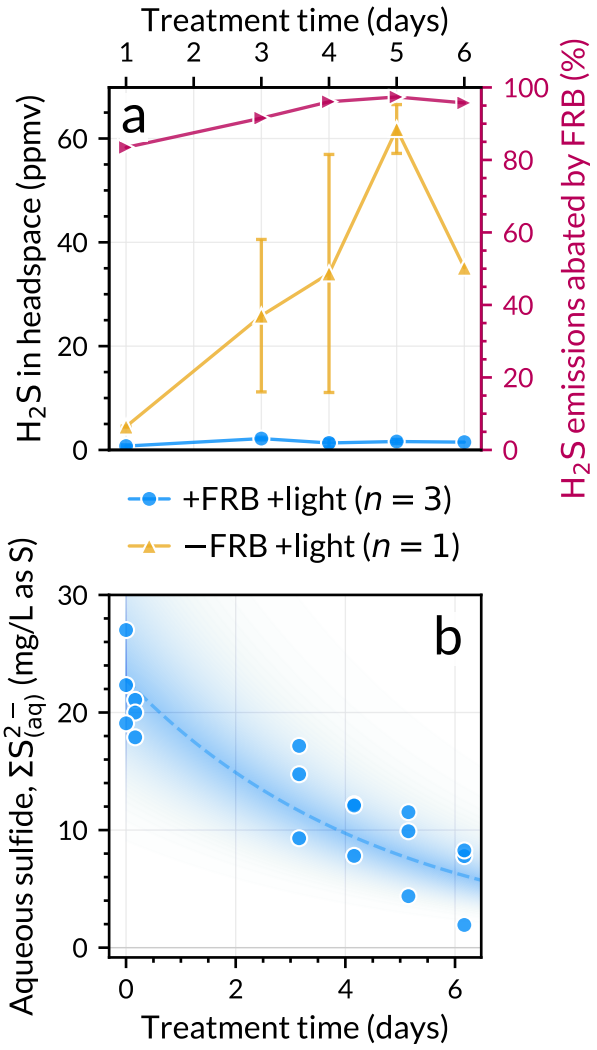

Figure 6 – a) Daily average headspace H2S concentrations and reduction between a sunlight exposed control (n=1 reactor) and treatment group (n=3 reactors). b) Field-scale photocatalytic degradation of aqueous sulfide in OSPW under the BPC layer. Error bars represent pooled test replicate variance (n=3) and analytical method uncertainty.

4.2.2 Reduced Sulfur Compound Bubble Interception

The objective of this test was to further investigate multiphase treatment, as prior experiments assumed transfer of sulfide to the headspace from the aqueous phase, however volatile sulfides can also be transported from the mature fluid tailings layer to the surface in biogas bubbles produced via

methanogenesis. To further prove the efficacy of the photocatalyst layer barrier it is necessary to also demonstrate the retention of emissions from multiphase sources. To this end, three closed-cell pilot-scale reactors were retrofitted with bubble diffusers and two experiments were performed with different bubble emission methods: air stripping with ambient air bubbled through an H_2S containing OSPW sample (Test #1), and H_2S gas (3%, balance N_2) bubbling in a similar manner (Test #2). Progress was monitored by visual observation (**Figure 7**), headspace H_2S measurement directly above the bubble stream, and aqueous phase sulfide sampling. The bubble diffusers were selected to produce bubbles of 0.1 to 0.5 mm diameter.

Test #1 had an initial aqueous concentration of 0.5 mg/L H_2S at pH of 9.5 (130 mg/L S^{2-}), and air stripping was performed at a volumetric gas flux of 46,262 mL/min/m^2, approximately 10,000x the expected total volumetric gas volume expected from the target tailings pond. During Test #1, the presence of the FRB layer resulted in an 87% reduction in H_2S emissions when compared to the control, primarily as a function of emission blocking (**Figure 8**). Test #2 had an initial aqueous concentration of 0.21 mg/L H_2S at a pH of 9.8 (127 mg/L S^{2-}), and gas was bubbled at a volumetric flux of 3,267 mL/min/m^2, approximately 710x the estimated flux from the target tailings pond. During this test H_2S emissions from the FRB layer were 89% less than the control (**Error! Reference source not found.**). While the bubbles eventually broke through the FRB layer, the layer cohesion had a capacitive effect in that bubbles were retained long enough for dissolution of the gaseous H_2S into the aqueous phase where it is subsequently oxidized by the photocatalyst. Additionally, following the gas bubble penetration, the FRB layer promptly reformed a cohesive layer, providing an advantage over traditional impermeable gas-blocking covers.

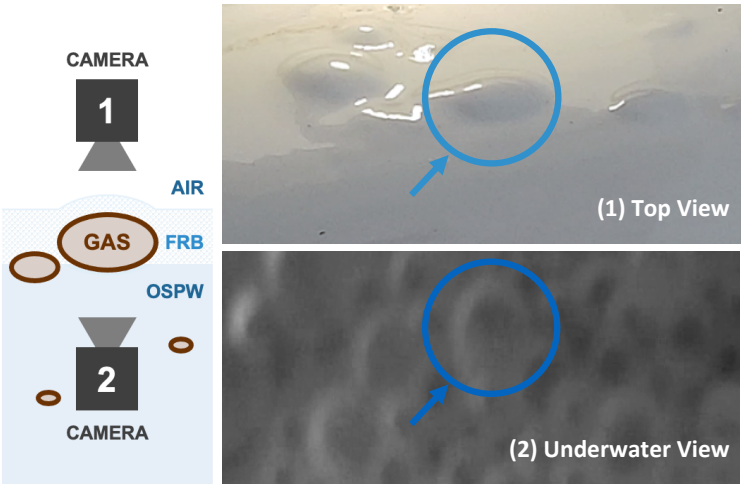

Figure 7 – Graphic of experimental setup for bubble observation (left) and bubbles shown above and below the OSPW level with the FRB layer (right).

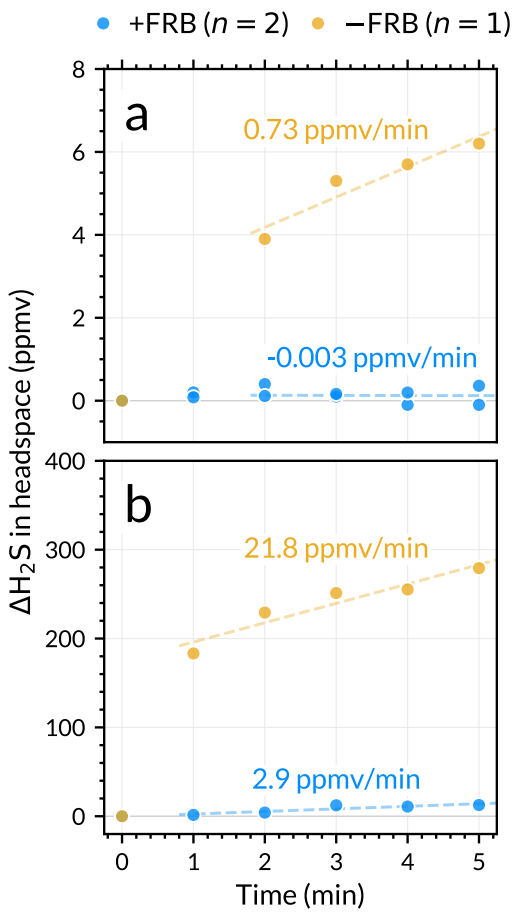

Figure 8 - a) Ambient air stripping bubble test results as measured over a burst period of air injection and b) H_2S gas (3%, balance N_2) bubbling test results.

4.3 Open-Tank System Results

The objective of the open-tank experiments was to evaluate the H_2S emissions reduction efficacy of the FRB layer in a larger pilot reactor with direct exposure to the local environmental conditions as a close simulation of actual tailings pond deployment. By not having a confined headspace, the possibility of back-transfer of H_2S into the aqueous phase in the closed-cell reactors can be eliminated. The H_2S flux from a section of the reactor covered with the FRB was compared to a bare surface section of the same reactor. The flux chamber analysis showed a 96% reduction in H_2S flux from the OSPW surface when covered by the FRB layer and compared to the bare surface (**Figure 9**). This experiment further validates the FRB layer efficacy to contain volatile sulfur compound emissions under realistic weather conditions for the reduction of emissions from an aqueous source.

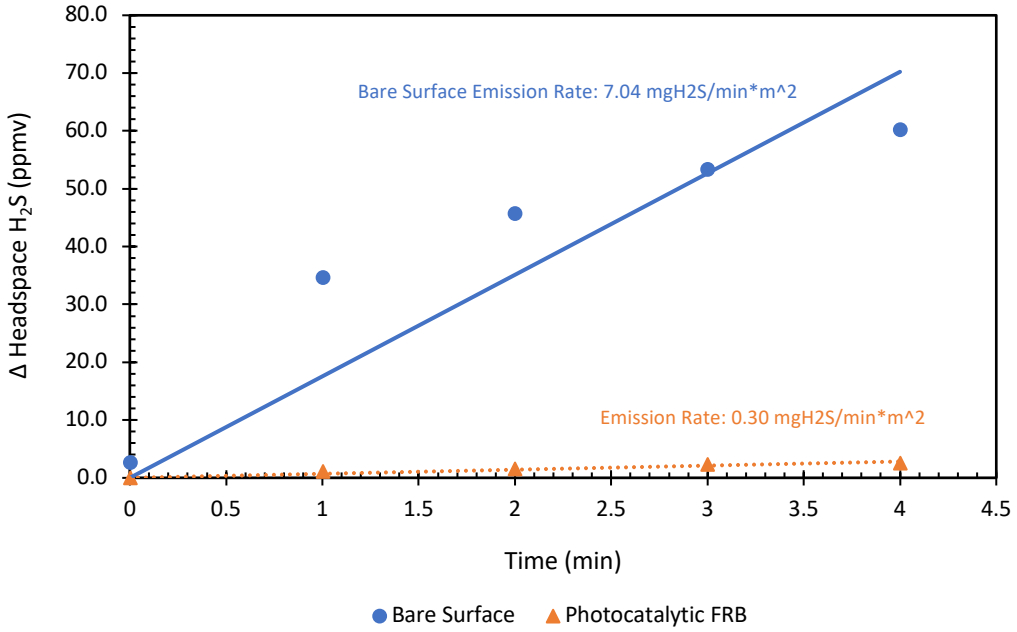

Figure 9 - Flux chamber and hand-held H_2S meter measurement of H_2S emissions from a bare and FRB covered surface measured after sodium sulfide addition.

4.4 Steady State Mass Transfer Modeling

Using the field-scale open tank experiments in Section 4.3, the diffusivity of aqueous sulfide ions in the FRB layer was derived (8.34×10^{-11} $m^2/s \pm 0.88 \times 10^{-11}$ m^2/s). Additionally, using this diffusivity coefficient, the internal FRB rate constant for the photocatalytic oxidation of sulfide was determined from the data obtained from the lab-scale experiments in Section **Error! Reference source not found.** and **Error! Reference source not found.** (1.93×10^{-4} $cm^2/mW/s \pm 0.13 \times 10^{-4}$ $cm^2/mW/s$). Using these experimentally derived parameters and the experimental lab-scale conditions, the sulfide concentration profile across the FRB layer was modelled (Figure 13). Additionally, using Henry's law, the theoretical H_2S concentration in the headspace of the lab-scale reactor was determined to be 5.9 ppm_v compared to the experimental value of 3.01 $ppm_v \pm 2.83$. While within the same order of magnitude, it is expected that the experimentally measured H_2S emissions will be lower than those predicted by the model due to gaseous-phase air oxidation that is not considered in the model. These results indicate that the steady-state model proposed in this study can accurately describe the mass transfer of volatile compounds through the FRB layer and further validates the effectiveness of the FRB layer for their retention and oxidative treatment.

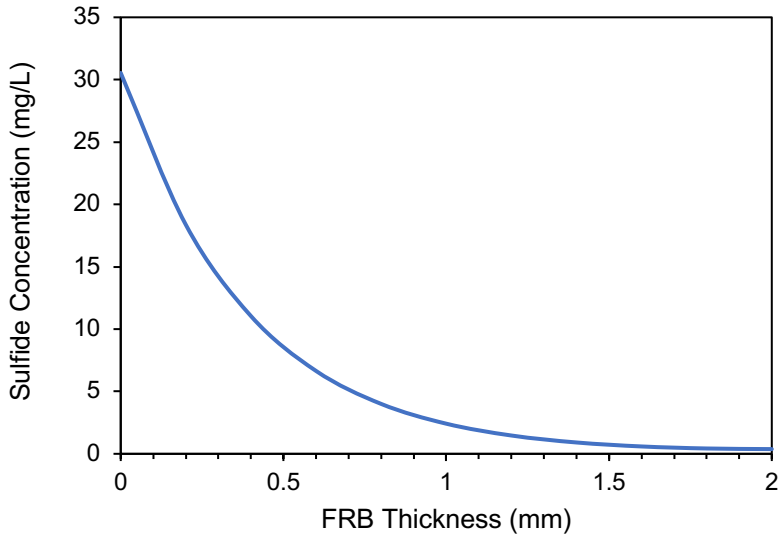

Figure 10 - Modeled sulfide concentration profile across the photocatalytic FRB assuming an FRB thickness of 1 cm, an irradiance of 3 mW/cm^2 and an initial aqueous sulfide concentration of 20 mg/L.

5.0 Conclusion

As a standalone process or part of a larger treatment system, the photocatalytic floating reactive barrier outlined in this work shows promise as a low-cost platform for retention and photocatalytic treatment of volatile reduced sulfur compounds. At the lab-scale, deployment of the FRB resulted in a reduction of H_2S emissions from sulfide-containing OSPW sources by up to 95%, coupled with simultaneous oxidization of the aqueous sulfide to non-volatile sulfate. This performance was further demonstrated at pilot-scale in a closed-cell reactor (550 L) with emissions blocking of up to 97% when compared to a control. Aqueous treatment was also demonstrated at field-scale, further enhanced by increased mass transfer due to natural diurnal temperature fluctuations. Additionally, the retention of H_2S emissions was successfully demonstrated for gas bubbles containing H_2S with an 89% decrease in the H_2S flux compared to a control. Further, under natural conditions in an open reactor, the efficacy of the photocatalytic FRB was validated with a 96% reduction in H_2S gas flux. Based on the results of this work, the capabilities of the photocatalytic FRB can be further extended to provide odour and greenhouse gas emissions reduction through the treatment and retention of additional volatile compounds including methane, volatile organic carbons, and ammonia.

6.0 Author information

T.M.C.L., Z.W.Y., and F.G. declare ownership stakes in H2nanO Inc., a company with financial interest in the subject matter of this work, as well as inventorship on a BPC patent application (PCT/IB2017/056505, US16/343,298) assigned to H2nanO. The other authors declare no potentially competing conflicts of interest.

7.0 References

[1] I. Devai and R. D. DeLaune, “Emission of Reduced Malodorous Sulfur Gases from Wastewater Treatment Plants,” *Water Environ. Res.*, vol. 71, no. 2, pp. 203–208, Mar. 1999, doi: 10.2175/106143098X121842.
[2] T. R. Carter, L. Fortner, M. E. Skuce, and F. J. Longstaffe, “Aquifer Systems in Southern Ontario: Hydrogeological Considerations for Well Drilling and Plugging,” p. 4.
[3] R. E. Jackson, M. B. Dusseault, S. Frape, W. Illman, T. Phan, and C. Steelman, “Investigating the Origin of Elevated H2S in Groundwater Discharge from Abandoned Gas Wells, Norfolk County, Ontario,” p. 5, 2020.
[4] B. K. McCabe, I. Hamawand, P. Harris, C. Baillie, and T. Yusaf, “A case study for biogas generation from covered anaerobic ponds treating abattoir wastewater: Investigation of pond performance and potential biogas production,” *Appl. Energy*, vol. 114, pp. 798–808, Feb. 2014, doi: 10.1016/j.apenergy.2013.10.020.
[5] Y. Wiyarno and S. Widyastuti, “Isolation and Identification Odorous Chemical Markers of Wastewater Poultry Slaughterhouse,” *Procedia Environ. Sci.*, vol. 23, pp. 400–406, Jan. 2015, doi: 10.1016/j.proenv.2015.01.057.
[6] T. Schmidt, P. Harris, S. Lee, and B. K. McCabe, “Investigating the impact of seasonal temperature variation on biogas production from covered anaerobic lagoons treating slaughterhouse wastewater using lab scale studies,” *J. Environ. Chem. Eng.*, vol. 7, no. 3, p. 103077, Jun. 2019, doi: 10.1016/j.jece.2019.103077.
[7] J. Blunden and V. P. Aneja, “Characterizing ammonia and hydrogen sulfide emissions from a swine waste treatment lagoon in North Carolina,” *Atmos. Environ.*, vol. 42, no. 14, pp. 3277–3290, May 2008, doi: 10.1016/j.atmosenv.2007.02.026.
[8] C. C. Small, S. Cho, Z. Hashisho, and A. C. Ulrich, “Emissions from oil sands tailings ponds: Review of tailings pond parameters and emission estimates,” *J. Pet. Sci. Eng.*, vol. 127, pp. 490–501, Mar. 2015, doi: 10.1016/j.petrol.2014.11.020.
[9] F. M. Holowenko, M. D. MacKinnon, and P. M. Fedorak, “Methanogens and sulfate-reducing bacteria in oil sands fine tailings waste,” vol. 46, p. 11, 2000.
[10] T. Siddique, P. M. Fedorak, M. D. MacKinnon, and J. M. Foght, “Metabolism of BTEX and Naphtha Compounds to Methane in Oil Sands Tailings,” *Environ. Sci. Technol.*, vol. 41, no. 7, pp. 2350–2356, Apr. 2007, doi: 10.1021/es062852q.
[11] A. Van Dongen *et al.*, “A Deep Look into the Microbiology and Chemistry of Froth Treatment Tailings: A Review,” *Microorganisms*, vol. 9, no. 5, p. 1091, May 2021, doi: 10.3390/microorganisms9051091.
[12] K. F. Gee, H. Y. Poon, Z. Hashisho, and A. C. Ulrich, “Effect of naphtha diluent on greenhouse gases and reduced sulfur compounds emissions from oil sands tailings,” *Sci. Total Environ.*, vol. 598, pp. 916–924, Nov. 2017, doi: 10.1016/j.scitotenv.2017.04.107.
[13] E. Ramos-Padrón *et al.*, “Carbon and Sulfur Cycling by Microbial Communities in a Gypsum-Treated Oil Sands Tailings Pond,” *Environ. Sci. Technol.*, vol. 45, no. 2, pp. 439–446, Jan. 2011, doi: 10.1021/es1028487.
[14] C. Davidson and D. Spink, “Alternate approaches for assessing impacts of oil sands development on air quality: A case study using the First Nation Community of Fort McKay,” *J. Air Waste Manag. Assoc.*, vol. 68, no. 4, pp. 308–328, Apr. 2018, doi: 10.1080/10962247.2017.1377648.
[15] S. N. Wren *et al.*, “Improving Insights on Air Pollutant Mixtures and Their Origins by Enhancing Local Monitoring in an Area of Intensive Resource Development,” *Environ. Sci. Technol.*, vol. 54, no. 23, pp. 14936–14945, Dec. 2020, doi: 10.1021/acs.est.0c06055.
[16] M. Dube *et al.*, “Recurrent Human Health Complaints Technical Information Synthesis: Fort McKay Area,” Alberta Energy Regulator & Alberta Health, Sep. 2016.

[17] A. Alonso-Tellez, D. Robert, N. Keller, and V. Keller, “A parametric study of the UV-A photocatalytic oxidation of H2S over TiO2,” *Appl. Catal. B Environ.*, vol. 115–116, pp. 209–218, Apr. 2012, doi: 10.1016/j.apcatb.2011.12.014.
[18] H. Nishikawa and Y. Takahara, “Adsorption and photocatalytic decomposition of odor compounds containing sulfur using TiO2/SiO2 bead,” *J. Mol. Catal. Chem.*, vol. 172, no. 1–2, pp. 247–251, Jul. 2001, doi: 10.1016/S1381-1169(01)00124-8.
[19] M. C. Canela, R. M. Alberici, and W. F. Jardim, “Gas-phase destruction of H2S using TiO2/UV-VIS,” *Joutnal Photochem. Photobiol. Chem.*, vol. 112, pp. 73–80, 1998.
[20] X. Hao, G. Hou, P. Zheng, R. Liu, and C. Liu, “H2S in-situ removal from biogas using a tubular zeolite/TiO2 photocatalytic reactor and the improvement on methane production,” *Chem. Eng. J.*, vol. 294, pp. 105–110, Jun. 2016, doi: 10.1016/j.cej.2016.02.098.
[21] Y.-C. Chung, K.-L. Ho, and C.-P. Tseng, “Treatment of High H_2S Concentrations by Chemical Absorption and Biological Oxidation Process,” *Environ. Eng. Sci.*, vol. 23, no. 6, pp. 942–953, Nov. 2006, doi: 10.1089/ees.2006.23.942.
[22] M. Lee *et al.*, “Pilot-Scale Testing of UV-A Light Treatment for Mitigation of NH3, H2S, GHGs, VOCs, Odor, and O3 Inside the Poultry Barn,” *Front. Chem.*, vol. 8, p. 613, Jul. 2020, doi: 10.3389/fchem.2020.00613.
[23] S. Kato, Y. Hirano, M. Iwata, T. Sano, K. Takeuchi, and S. Matsuzawa, “Photocatalytic degradation of gaseous sulfur compounds by silver-deposited titanium dioxide,” *Appl. Catal. B Environ.*, vol. 57, no. 2, pp. 109–115, Apr. 2005, doi: 10.1016/j.apcatb.2004.10.015.
[24] K. Vikrant, K.-H. Kim, and A. Deep, “Photocatalytic mineralization of hydrogen sulfide as a dual-phase technique for hydrogen production and environmental remediation,” *Appl. Catal. B Environ.*, vol. 259, p. 118025, Dec. 2019, doi: 10.1016/j.apcatb.2019.118025.
[25] T. Leshuk, H. Krishnakumar, D. de Oliveira Livera, and F. Gu, “Floating Photocatalysts for Passive Solar Degradation of Naphthenic Acids in Oil Sands Process-Affected Water,” *Water*, vol. 10, no. 2, p. 202, Feb. 2018, doi: 10.3390/w10020202.
[26] T. Leshuk *et al.*, “Petroleomic analysis of the treatment of naphthenic organics in oil sands process-affected water with buoyant photocatalysts,” *Water Res.*, vol. 141, pp. 297–306, Sep. 2018, doi: 10.1016/j.watres.2018.05.011.
[27] D. W. Blowes, C. J. Ptacek, S. G. Benner, C. W. T. McRae, T. A. Bennett, and R. W. Puls, “Treatment of inorganic contaminants using permeable reactive barriers,” *J. Contam. Hydrol.*, vol. 45, no. 1–2, pp. 123–137, Sep. 2000, doi: 10.1016/S0169-7722(00)00122-4.
[28] R. D. Ludwig, R. G. McGregor, D. W. Blowes, S. G. Benner, and K. Mountjoy, “A Permeable Reactive Barrier for Treatment of Heavy Metals,” *Ground Water*, vol. 40, no. 1, pp. 59–66, Jan. 2002, doi: 10.1111/j.1745-6584.2002.tb02491.x.
[29] A. Houas, H. Lachheb, M. Ksibi, E. Elaloui, C. Guillard, and J.-M. Herrmann, “Photocatalytic degradation pathway of methylene blue in water,” *Appl. Catal. B Environ.*, vol. 31, no. 2, pp. 145–157, May 2001, doi: 10.1016/S0926-3373(00)00276-9.
[30] I. K. Konstantinou and T. A. Albanis, “Photocatalytic transformation of pesticides in aqueous titanium dioxide suspensions using artificial and solar light: intermediates and degradation pathways,” *Appl. Catal. B Environ.*, vol. 42, no. 4, pp. 319–335, Jun. 2003, doi: 10.1016/S0926-3373(02)00266-7.
[31] K. V. Kumar, K. Porkodi, and F. Rocha, “Langmuir–Hinshelwood kinetics – A theoretical study,” *Catal. Commun.*, vol. 9, no. 1, pp. 82–84, Jan. 2008, doi: 10.1016/j.catcom.2007.05.019.
[32] A. K. Gupta, A. Pal, and C. Sahoo, “Photocatalytic degradation of a mixture of Crystal Violet (Basic Violet 3) and Methyl Red dye in aqueous suspensions using Ag+ doped TiO2,” *Dyes Pigments*, vol. 3, no. 69, pp. 224–232, 2006, doi: 10.1016/j.dyepig.2005.04.001.

[33] I. Poulios, E. Micropoulou, R. Panou, and E. Kostopoulou, “Photooxidation of eosin Y in the presence of semiconducting oxides,” *Appl. Catal. B Environ.*, vol. 41, no. 4, pp. 345–355, Mar. 2003, doi: 10.1016/S0926-3373(02)00160-1.
[34] T. Sauer, G. Cesconeto Neto, H. J. José, and R. F. P. M. Moreira, “Kinetics of photocatalytic degradation of reactive dyes in a TiO2 slurry reactor,” *J. Photochem. Photobiol. Chem.*, vol. 149, no. 1, pp. 147–154, Jun. 2002, doi: 10.1016/S1010-6030(02)00015-1.
[35] I. K. Konstantinou and T. A. Albanis, “TiO2-assisted photocatalytic degradation of azo dyes in aqueous solution: kinetic and mechanistic investigations: A review,” *Appl. Catal. B Environ.*, vol. 49, no. 1, pp. 1–14, Apr. 2004, doi: 10.1016/j.apcatb.2003.11.010.
[36] “APHA Method 4500-S2-: Standard Methods for the Examination of Water and Wastewater,”
[37] P. K. Dasgupta, Kymron. DeCesare, and J. C. Ullrey, “Determination of atmospheric sulfur dioxide without tetrachloromercurate(II) and the mechanism of the Schiff reaction,” *Anal. Chem.*, vol. 52, no. 12, pp. 1912–1922, Oct. 1980, doi: 10.1021/ac50062a031.
[38] Y. Li and M. Zhao, “Simple methods for rapid determination of sulfite in food products,” *Food Control*, vol. 17, no. 12, pp. 975–980, Dec. 2006, doi: 10.1016/j.foodcont.2005.07.008.
[39] “APHA Method 4500-SO42: Standard Methods for the Examination of Water and Wastewater,”
[40] K. Whaley-Martin *et al.*, “A Mass-Balance Tool for Monitoring Potential Dissolved Sulfur Oxidation Risks in Mining Impacted Waters,” *Mine Water Environ.*, vol. 39, no. 2, pp. 291–307, Jun. 2020, doi: 10.1007/s10230-020-00671-0.
[41] G. A. Lawrence, P. R. B. Ward, and M. D. MacKinnon, “Wind-wave-induced suspension of mine tailings in disposal ponds – a case study,” *Can. J. Civ. Eng.*, vol. 18, no. 6, pp. 1047–1053, Dec. 1991, doi: 10.1139/l91-127.
[42] G. A. Lawrence, E. W. Tedford, and R. Pieters, “Suspended solids in an end pit lake: potential mixing mechanisms,” *Can. J. Civ. Eng.*, vol. 43, no. 3, pp. 211–217, Mar. 2016, doi: 10.1139/cjce-2015-0381.
[43] K. A. Dompierre and S. L. Barbour, “Characterization of physical mass transport through oil sands fluid fine tailings in an end pit lake: a multi-tracer study,” *J. Contam. Hydrol.*, vol. 189, pp. 12–26, Jun. 2016, doi: 10.1016/j.jconhyd.2016.03.006.
[44] Y. You, R. M. Staebler, S. G. Moussa, J. Beck, and R. L. Mittermeier, “Methane emissions from an oil sands tailings pond: a quantitative comparison of fluxes derived by different methods,” *Atmospheric Meas. Tech.*, vol. 14, no. 3, pp. 1879–1892, Mar. 2021, doi: 10.5194/amt-14-1879-2021.